Impurity transport studies on Wendelstein 7-X by Tracer-Encapsulated Solid Pellets

R. Bussiahn[1], N. Tamura[2], K.J. McCarthy[3], T. Andreeva[1], J. Brunner[1], B. Buttenschön[1], A. Dinklage[1], B. Geiger[4], J. Geiger[1], G. Fuchert[1], A. Langenberg[1], N. Pablant[5], K. Rhabarnia[1], C. Swee[4], Th. Wegner[1] and the W7-X team[1]

[1] *Max-Planck-Institut für Plasmaphysik, Greifswald, Germany;* [2] *National Institute for Fusion Science, Toki, Japan;* [3] *Laboratorio Nacional de Fusión, Ciemat, Madrid, Spain;* [4] *University of Wisconsin, Madison, WI, USA,* [5] *Princeton Plasma Physics Laboratory, Princeton, NJ, USA*

Shortly before the start of the OP1.2b operation phase of the stellarator Wendelstein 7-X, a new Tracer-Encapsulated Solid Pellet (TESPEL) injection system was installed [1, 2]. TESPEL has been developed at NIFS, Japan [3] and has proven successfully as a complementary tool to Laser-Blow-Off (LBO) for impurity transport studies. Contrary to LBO - which deposits tracers close to the plasma edge that are subsequently transported and spread out into the plasma, TESPEL can release the embedded impurity tracers instantly in the plasma core, within a well defined spatial volume of a few cm^3, once the protective polystyrene shell has been ablated.

Comparing the temporal dynamics of the shell ablation with a neutral gas shielding model gives good agreement (figure 1). Despite some differences between the shapes of the ablation signal and the calculated rate, the shell ablation end as the important quantity is very well reproduced. As seen from fast-frame camera images of the shell ablation cloud, the TESPEL trajectory through the plasma does not suffer any deflections [5]. This permits localizing the deposited tracer in the plasma by a simple time-of-flight estimation.

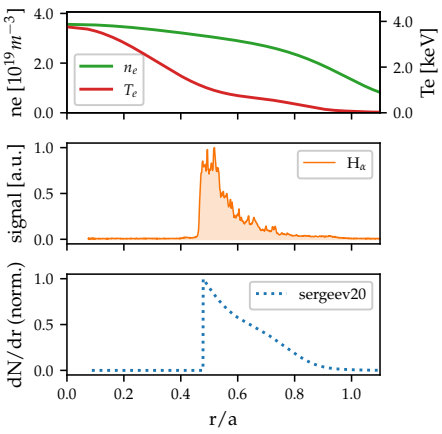

Figure 1: *Kinetic profiles, shell ablation signal and ablation rate (calculated according to equation 20 in [4]) for W7-X #20180906.38.*

Correlating the TESPEL speed - measured from times when the pellet passes two laser light-barriers - with the start and end of the tracer ablation signal (figure 2), gives the travelled distance after passing one of the light barriers. A reliable determination of the tracer ablation start and end time was only possible by comparing the differential and relative signals (figures 2 (b) and 2 (c)) of the shell and tracer channel. By mapping the travelled distances onto the trajectory coordinates and taking into account the magneto-hydrodynamic equilibrium (from VMEC reference

calculations), the release of the tracer can be localised in the r_{eff}/a-space (figure 3).

For impurity transport studies by means of the code STRAHL, the precise localisation of TESPEL induced tracers is a critical input parameter. Figure 4 shows the electron temperature dependent penetration depth results for all TESPEL injections in Wendelstein 7-Xs operation phase 1.2b. The trend lines indicate a linear dependency of the TESPEL penetration depth from the electron temperature.

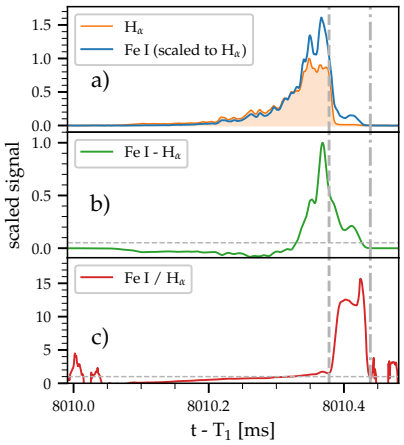

Figure 2: *Tracer separation (W7-X #20180906.38). a) shell and tracer ablation signals, b) differential signal, c) signal quotient. The vertical bars indicate the tracer ablation start and end times.*

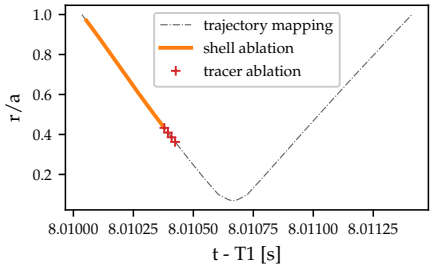

Figure 3: *Mapping of the data from figure 2 onto the nominal injection axis.*

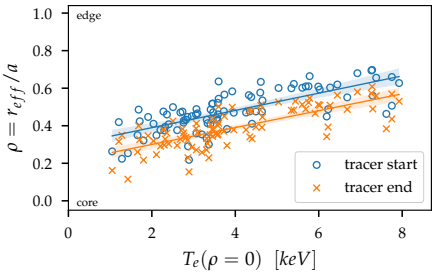

Figure 4: *Electron temperature dependent TESPEL penetration depth for W7-X OP1.2b experiments.*

The different ways in which tracers are released after injection by LBO or TESPELs is manifested in the line emissions from the the various ionisation stages (cf. figure 5) as observed by vacuum ultraviolet spectroscopy (HEXOS) and high resolution X-ray imaging spectrometry (HR-XIS). For LBO, the tracers are affected by subsequently rising electron density and temperature as they are transported from the edge into the core plasma. While the lowest stages (e.g. Fe XV) are very quickly ionised, it takes increasingly longer times for higher stages to be reached. This directly reflects the involved inward transport processes, tracers need to enter radial regions with sufficiently high electron temperature before they can be ionised from lower energetic states. So the steepness of the leading edge in the LBO signals becomes more and more shallow, the higher the related ionisation stage is. In contrast, tracers released deep in the core plasma are affected by high electron density and temperature from the very beginning. Therefore the ionisation into higher stages happens almost immediately. So the change in the leading edge steepness of the emission line timetraces is less pronounced than for LBO injections. Then almost immediately after the inital ionisation, the signal intensity for TESPEL injected tracers in the lower stages drops again due to ionisation into higher stages. For the lower-most (c.f. Fe XV + Fe XX in figure 5) stages, a second

peak appears after a few 10 ms. This reflects recombination processes in which these stages are repopulated as they are transported outwards and reach regions of lower temperatures again. As soon as the outward transport dominates, the signals decay exponentially, independently of the ways in which tracers were delivered. In the semi-logarithmic plot, this is seen as linearly decreasing curves for all obseved lines.

Fitting this signal part gives the characteristic time constant τ_{imp} of the outward directed transport. As an example, figure 6 shows the derived impurity transport times as function of the electron cyclotron resonance heating (ECRH) power. As the trend line in the double logarithmic plot implies is τ_{imp} inversely proportional to P^{α}_{ECRH}. While most of the experiments, conducted under moderate to high ECRH power conditions led to transport times well below 200 ms, a few experiments with low ECR heating power exhibit significantly enlarged values for τ_{imp}. This might point to impurity accumulation effects, becoming increasingly import with lower ECR heating power.

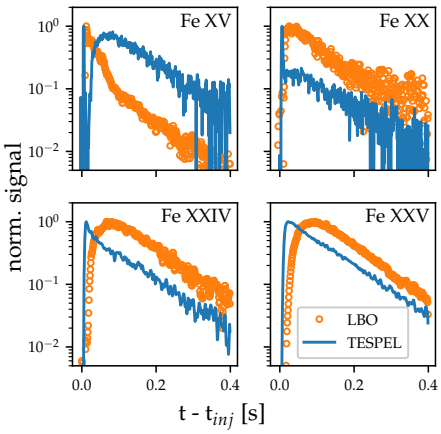

Figure 5: *Line emission of different ionisation stages for LBO (t_{inj} = 7.0 s) and TESPEL injections (t_{inj} = 8.0 s) in W7-X #20180906.38.*

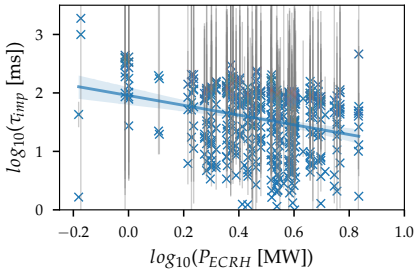

Figure 6: *Impurity transport time as function of the ECR heating power.*

While impurity transport times can be seen as a good indicator for general trends, a robust statement towards underlying transport effects requires a detailed analysis. The code STRAHL [6], calculating the radial transport and the emission of impurities in the plasma bulk, is a widely used tool for this purpose. Recently, STRAHL has been employed to derive transport parameters for LBO injections in W7-X [7]. In a similar approach, the emission lines of different ionized Fe species, detected by HEXOS and HR-XIS were taken as references to compare them with STRAHL-calculated emissivities while varying the input diffusion and convection profiles iteratively. In a first attempt, only slightly adapting the fitting procedure that has been employed for LBO injections, only a poor rendering of some individual features beeing present in the emission lines of TESPEL injected tracers could be achieved. In particular, the very dynamic phase immediately after the tracer release (c.f. figure 5) was not properly represented in the modelled time-dependent emissivity curves.

One of the difficulties with adapting STRAHL fitting routines for TESPEL analysis is the

different way, as discussed above, in which the tracer is initially released. For this reason, the general applicability of STRAHL for TESPEL is tested under simplified conditions. For this purpose, a basic fitting routine - neglecting contributions from convective transport (v=0) and only varying the injection time - was used to calculate relative line emissivities for different radially constant diffusion values (source location: experimental value) and different spatial locations (for $D_{const} = 0.5\ m^2 s^{-1}$) of the tracer source profile.

Figure 7 shows the reduced χ^2 ($\chi^2_r = \chi^2/N$, N: number of data points) values for these tests, indicating best fit results for $D_{const} = 0.5\ m^2 s^{-1}$ and a source location of $r_{eff}/a \approx 0.4$. The latter matches very well with the experimentally determined tracer

deposition range as shown in figure 4. A comparison of experimental line emissions and the related results of STRAHL-calculations for these best input parameters is shown in figure 8. The STRAHL results coincide already fairly well with the experimental data, which reassures again the reliability of the applied tracer localization method. Additionally, it confirms findings from LBO injections on the important role of anomalous diffusion in W7-X [7], as the determind value of the diffusion coefficient with $D = D_{nc} + D_a = 0.5\ m^2 s^{-1}$ would require a contribution of anomalous diffusion D_a which is a few times tens higher than those of the neoclassical diffusion D_{nc}.

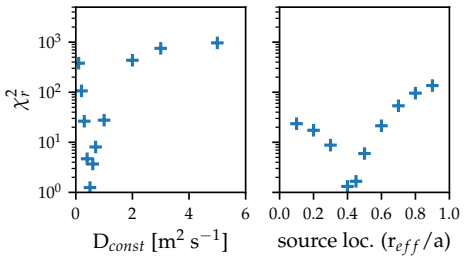

Figure 7: *Reduced χ^2 values, indicating the fit quality while varying the diffusion coefficient (left) and the source location (right).*

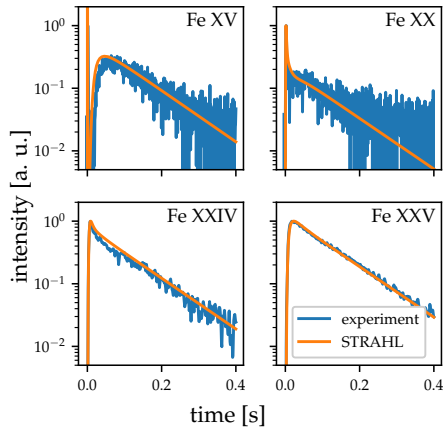

Figure 8: *Comparison between the experimentally determined line emission of ionized iron states and relative emissivities, calculated by STRAHL.*

References

[1] R. Bussiahn et.al., Rev. Sci. Instrum. **89**, 10K112 (2018)
[2] R. Laube et.al., Fusion Eng. Des., **150**, 111259 (2020)
[3] S. Sudo, J. Plasma Fusion Res. **69**, 1349 (1993).
[4] V. Yu. Sergeev et.al., Plasma. Phys. Rep. **32**, 363 (2006)
[5] G. Kocsis et.al., Nucl. Fusion **61**, 016006 (2021)
[6] K. Behringer, JET-R–87-08, (1987)
[7] B. Geiger et.al., Nucl. Fusion **59**, 046009 (2019)

"This work has been carried out within the framework of the EUROfusion Consortium and has received funding from the Euratom research and training programme 2014-2018 and 2019-2020 under grant agreement No 633053. The views and opinions expressed herein do not necessarily reflect those of the European Commission."